Synthesis, Structure, and Properties of Ionic Thermoplastic Elastomers Based on Maleated Ethylene/Propylene Copolymers

M. A. J. van der Mee,[†,‡] R. M. A. l'Abee,[†,‡] G. Portale,[‡,§] J. G. P. Goossens,*[,†,‡] and M. van Duin[||]

Laboratory of Polymer Technology, Department of Chemical Engineering and Chemistry, Eindhoven University of Technology, P.O. Box 513, 5600 MB Eindhoven, The Netherlands; Dutch Polymer Institute, P.O. Box 902, 5600 AX Eindhoven, The Netherlands; Netherlands Organization for Scientific Research (NWO), DUBBLE CRG, ESRF, 6 rue Jules Horowitz, BP 220, F-38043 Grenoble Cédex 9, France; and DSM Research, P.O. Box 18, 6160 MD Geleen, The Netherlands

Received July 18, 2007; Revised Manuscript Received May 28, 2008

ABSTRACT: Ionic thermoplastic elastomers with dicarboxylate functionalities were obtained via neutralization of high-molecular-weight hydrolyzed maleated EPM rubber (MAn-*g*-EPM) with potassium (K^+) and zinc (Zn^{2+}) acetate. The lower reactivity of the second of two adjacent carboxylic acid groups after neutralization of the first group prevents neutralization beyond 50% with monovalent K^+ cations, while the remaining positive charge for divalent Zn^{2+} cations enables further neutralization. Small-angle X-ray scattering (SAXS) showed the presence of microphase-separated domains already for the MAn-*g*-EPM precursor as well as for the K- and Zn-ionomers. The type of cation has an important influence on the final morphology and properties. K-ionomers display a better phase separation than the corresponding Zn-ionomers. The SAXS data strongly suggest the presence of small, isolated multiplets, randomly dispersed within the matrix, next to the microphase-separated domains. This contribution is incorporated in the classical Yarusso−Cooper model together with the polydispersity of the domain size, and a very good fitting of the SAXS patterns is obtained. Neutralization causes the ionic network to persist up to higher temperatures, while the overall network density remains unaffected. The tensile properties and elasticity improve with increasing degree of neutralization (*DN*), showing significantly better properties for the K-ionomers than for the Zn-ionomers.

Introduction

Ionomers are polymers that contain a relatively small amount (up to 15 mol %) of ionic groups pendant to or incorporated in the polymer backbone.[1−3] The ionic groups are usually obtained via partial or full neutralization of acid groups, mainly carboxylic or sulfonic acids, with metal salts. It is well established that the ionic groups tend to form microphase-separated ionic aggregates within the nonionic matrix due to the large polarity difference between the ionic groups and the less polar backbone.[1−3] The existence of these aggregates has been proven for many ionomers, mainly by using small-angle X-ray and neutron scattering (SAXS and SANS). A typical feature of SAXS profiles of ionomers is the so-called "ionic" peak, usually observed at q values around 0.1−0.4 Å^{-1}, where q is the modulus of the scattering vector ($q = (4\pi/\lambda) \sin \theta$, where λ is the wavelength and 2θ is the scattering angle). Many structural models have been proposed to explain the morphology of ionomers,[4−9] but there is still no general consensus on the correct model. The ionic aggregates act as physical cross-links and are responsible for the unique physical, mechanical, and rheological properties of ionomers.

The melt processability of ionomers is related to the increased mobility of the ionic pairs inside the aggregates at elevated temperatures. Therefore, ionomers based on noncrystalline polymers with a low T_g can be used as "ionic" thermoplastic elastomers (TPEs), if the ionic associations are sufficiently weakened at the processing temperatures.[10−12] One example is metal-neutralized sulfonated EPDM, where EPDM is a terpolymer of ethylene, propylene, and a diene monomer. The mechanical properties of EPDM are significantly improved upon the introduction of small amounts of zinc sulfonate groups and can even approach those of vulcanized EPDM.[13−15] However, the ionic interactions are too strong at conventional processing temperatures, resulting in very high melt viscosities. Lundberg et al.[16] showed that the ionic associations in sulfonated ionomers are much stronger than in their carboxylated analogues, resulting in melt viscosities that are 2−3 orders of magnitude higher. An additional disadvantage of sulfonated ionomers is that full neutralization is required, since residual sulfonic acid groups may thermally degrade at elevated temperatures. Therefore, carboxylated ionomers are preferred for practical applications.

Other attempts to prepare ionic TPEs also resulted in ionomers with too high melt viscosities.[11,17,18] In most cases, the ionomer precursor was an elastomer of relatively high molecular weight. During previous work in our group, the use of maleated ethylene/propylene copolymers (MAn-*g*-EPM) with a relatively low molecular weight as ionomer precursors was proposed to obtain ionomers with acceptable processing properties.[19−21] The ionomers were prepared via hydrolysis of the grafted maleic anhydride (MAn) groups to the corresponding dicarboxylic acids, followed by neutralization with metal acetates, resulting in ionomers with dicarboxylate functionalities. The morphology of these ionomers was studied by using SAXS and solid-state NMR.[20] An evaluation of several structural models showed that the Yarusso−Cooper (Y−C) model[8] was the best model for the interpretation of the SAXS results.[19] The size of the domains in these MAn-*g*-EPM-based ionomers and, consequently, the number of ionic groups within the domains were significantly larger than for other types of ionomers, such as sodium- or zinc-neutralized ethylene−methacrylic acid copolymers.[20] The melt viscosities of these low-molecular-weight ionomers were still relatively high, most probably related to the high degrees of

* Corresponding author: e-mail j.g.p.goossens@tue.nl, Tel +31 40 2473899, Fax +31 40 2436999.
[†] Eindhoven University of Technology.
[‡] Dutch Polymer Institute.
[§] Netherlands Organization for Scientific Research (NWO).
[||] DSM Research.

10.1021/ma8007509 CCC: $40.75
Published on Web 06/21/2008

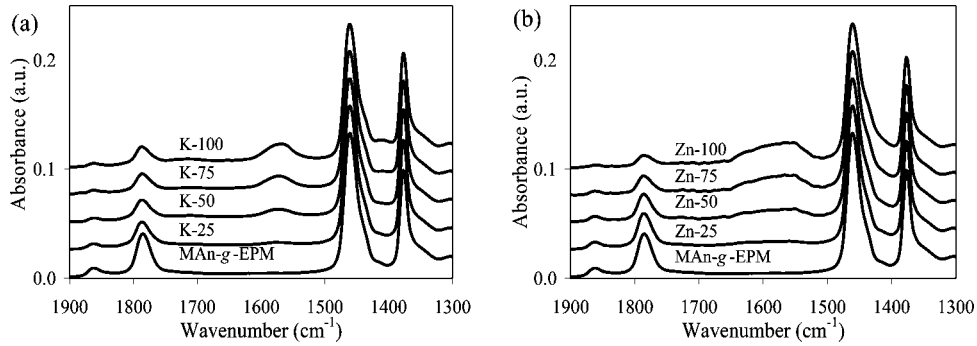

Figure 1. FTIR spectra for MAn-*g*-EPM and (a) K-ionomers and (b) Zn-ionomers with various DN_t after drying for 1 h at 170 °C. The spectra are shifted vertically for clarity.

grafting (DG) that were necessary to obtain acceptable mechanical properties.

Therefore, in the current study, a different MAn-*g*-EPM precursor is evaluated with a higher, but still relatively low, molecular weight (M_n = 40 kg/mol) and a lower DG (2.1 wt %) compared to those of the low-molecular-weight precursor used in the previous studies,[19–21] which had a M_n of 11 kg/mol and a DG of 7.3 wt %. Both precursors have a comparable average number of grafted MAn groups per EPM chain (Ω), which is calculated using

$$\Omega = \frac{M_{EPM} DG \times 1000}{M_{MAn} \times 100} \tag{1}$$

where M_{EPM} is the molecular weight of the precursor (kg/mol) and M_{MAn} is the molecular weight of the grafted maleic anhydride (99 g/mol). This results in Ω = 8.1 for the low-molecular-weight MAn-*g*-EPM and Ω = 8.5 for the current MAn-*g*-EPM precursor, which implies that the molecular weight between functional groups is ≈4 times larger.

The MAn-*g*-EPM precursor is neutralized to various targeted degrees of neutralization (*DN*) with two different cations, namely monovalent potassium (K^+) and divalent zinc (Zn^{2+}). The formation of the ionomers and the actual *DN* are studied by using Fourier transform infrared (FTIR) spectroscopy. The effects of *DN* and the type of metal cation on the morphology are studied with SAXS and dynamic mechanical thermal analysis (DMTA) as well as their effects on the rubber properties, i.e., elasticity and tensile properties. The SAXS results are interpreted with a modified Y−C model[8] to better describe the morphology. To support the morphological picture, the effect of water absorption was also studied, since ionomers are generally sensitive to water absorption due to the hydrophilic ionic groups, which tend to attract polar species, such as water molecules. Water, preferentially absorbed within the ionic-rich domains, mainly affects the domain structure.[22,23] Additionally, a comparison of the morphology and the properties is made with the low-molecular-weight ionomers from the previous work.[19]

Experimental Section

Materials. Maleated ethylene/propylene copolymer (MAn-*g*-EPM, 49 wt % ethylene, 49 wt % propylene, 2.1 wt % maleic anhydride (MAn), M_n = 40 kg/mol, M_w = 90 kg/mol) and the parent EPM (50 wt % ethylene, 50 wt % propylene, M_n = 40 kg/mol, M_w = 90 kg/mol) were provided by DSM Elastomers. The MAn-*g*-EPM precursor was dried for 1 h at 170 °C under reduced pressure with a low nitrogen flow prior to use to convert all carboxylic acid groups, formed upon hydrolysis, back to anhydride. Zinc acetate dihydrate ($ZnAc_2$, Fluka), potassium acetate (KAc, Aldrich), potassium hydroxide (KOH, Aldrich), toluene (Biosolve), and 2-propanol (Biosolve) were used as received.

Preparation of the Ionomers. Typically, 25 g of MAn-*g*-EPM was dissolved in a mixture of 225 g of toluene and 25 g of 2-propanol at 80 °C. After complete dissolution of the precursor, 10 g of an aqueous solution containing the required amount of metal salt, i.e., $ZnAc_2$, KAc, or KOH, was added, and the two-phase mixture was stirred for 15 min at 80 °C. Approximately 50 g of solvent was distilled off to remove the excess water. Then, 50 g of the toluene/2-propanol solvent mixture was added to the viscous system, followed by homogenization for 15 min at 80 °C. This cycle of evaporation and subsequent solvent addition was repeated as long as droplets of water were visible inside the toluene phase. The resulting gel was dried under a nitrogen flow for several days at room temperature, followed by drying for 24 h at 100 °C.

The targeted degree of neutralization (DN_t) is calculated using

$$DN_t = \frac{\nu m_{MAc} \times 1000}{M_{MAc} \chi m_{precursor}} \times 100\% \tag{2}$$

where ν is the valency of the metal ion, m_{MAc} is the mass of metal acetate added (g), M_{MAc} is the molecular weight of the metal acetate (g/mol), $m_{precursor}$ is the mass of MAn-*g*-EPM (g), and χ is the acid content, which is calculated using

$$\chi = \frac{DG}{100} \frac{1000}{M_{MAn}} \times 2 = 0.424 \text{ equiv acid/kg rubber} \tag{3}$$

The samples are designated as *M*-DN_t, where *M* is the type of cation.

For the study on the effect of water absorption, the ionomers were immersed in water for several days. The water uptake was gravimetrically determined from the change in weight before and after the water treatment.

Compression Molding. The materials were dried for 1 h at 170 °C under reduced pressure with a low nitrogen flow prior to compression molding. Samples were compression molded between Teflon sheets for 20 min in a Collin press at 150 °C for EPM and MAn-*g*-EPM and at 200 °C for the ionomers.

Fourier Transform Infrared (FTIR) Spectroscopy. Samples were measured on a BioRad Excalibur 3000 spectrometer equipped with a Specac Golden Gate attenuated total reflection (ATR) setup in a spectral range from 650 to 4000 cm^{-1} at a resolution of 4 cm^{-1}, coadding 35 scans. The experimental degree of neutralization (DN_{exp}) is calculated from the integrated intensity of the antisymmetric carbonyl (C═O) stretching vibration band of the anhydride groups at 1785 cm^{-1} (A_{1785}), using the intensity of the methyl rocking vibration band at 723 cm^{-1} originating from the EPM backbone (A_{723}) as internal reference:

$$DN_{exp} = \left(1 - \left(\frac{(A_{1785}/A_{723})_{ionomer}}{(A_{1785}/A_{723})_{precursor}}\right)\right) \times 100\% \tag{4}$$

Small-Angle X-ray Scattering (SAXS). SAXS experiments were performed on compression-molded samples at the DUBBLE beamline (BM26B) at the European Synchrotron Radiation Facility (ESRF) in Grenoble (France).[24] The data were collected using a 2D multiwire gas-filled detector with pixel array dimensions of 512 × 512. The detector was positioned 2 m away from the sample, and the *q* scale was calibrated using the position of diffracted peaks

from a standard silver behenate powder. The exposure time for each sample was 300 s, and a wavelength of 1.2 Å was used. The experimental data were corrected for the background scattering and transformed into 1D plots by azimuthal angle integration using the FIT2D program developed by Dr. Hammersley (ESRF). The resulting intensities were scaled to absolute intensity (in cm^{-1}) as a function of q using a Lupolen standard, which was measured via the same procedure. Finally, the data were converted to the normalized intensity per unit sample volume $I(q)/[I_e(q)V]$ (in $Å^{-3}$).

The samples were kept under vacuum overnight at 150 °C before the measurements, while the wet samples were prepared by immersion in water for several days. The wet samples were measured after removing the water from the surface by a paper tissue. During the acquisition of the SAXS data, no significant changes in morphology occurred due to the slow water absorption kinetics.

Dynamic Mechanical Thermal Analysis (DMTA). Rectangular samples with dimensions of 10 × 3 × 1 mm were measured over a temperature range from −100 to 250 °C at a heating rate of 3 °C/min and a frequency of 1 Hz on a DMA Q800 (TA Instruments) with film tension clamps.

Tensile Testing. Dumbbell-shaped tensile bars with dimensions of 35 × 2 × 1 mm were punched from compression-molded films. Tensile tests were performed at room temperature with a constant speed of 0.5 mm/s on a Zwick Z010 tensile tester equipped with a force cell of 20 N using TestXpert v7.11 software. All materials were tested in at least 5-fold.

Compression Set (*CS*). Cylindrical samples with a diameter of 13 mm and a thickness of ≈6 mm were compressed for 22 h between two parallel plates with a linear deformation of 25% at room temperature (CS_{23}) or at 70 °C (CS_{70}). *CS* was determined after a relaxation time of 30 min at room temperature by using the following equation:

$$CS = (t_0 - t_i)/(t_0 - t_n) \times 100\% \quad (5)$$

where t_n is the thickness of the spacer and t_0 and t_i are the initial and final sample thickness, respectively.

Results and Discussion

Preparation of the Ionomers. The ionomer precursor MAn-*g*-EPM is neutralized with KAc and $ZnAc_2$ to different targeted degrees of neutralization (DN_t). FTIR spectroscopy is a suitable technique to study the actual neutralization of MAn-*g*-EPM, since the position and the intensity of the carbonyl (C═O) stretching vibration bands change upon neutralization. The FTIR spectrum of the dried precursor MAn-*g*-EPM in Figure 1 shows two absorption bands characteristic for saturated, cyclic anhydrides at 1785 cm^{-1} (strong) and 1865 cm^{-1} (weak), originating from the antisymmetric and symmetric C═O stretching vibrations, respectively.[25] The strong bands at 1460 and 1380 cm^{-1}, which originate from the overlapping antisymmetric CH_3 bending and CH_2 scissoring and the symmetric CH_3 bending vibrations of the EPM backbone, respectively,[25] remain unchanged upon neutralization. The intensities of the anhydride bands decrease upon neutralization (Figure 1), while a new band at 1560 cm^{-1} appears for the K-ionomers and two overlapping bands around 1630 and 1560 cm^{-1} for the Zn-ionomers. These new bands are attributed to the C═O stretching vibration(s) of the metal-carboxylates.[17,25,26] The difference in the (number of) carboxylate bands between the K- and Zn-ionomers is related to differences in the coordination around the metal cations.[26]

Figure 2 shows the experimental *DN* (DN_{exp}), which was determined from the FTIR spectra according to eq 4, as a function of DN_t. All ionomers were dried for 1 h at 170 °C prior to the FTIR experiments to convert all remaining carboxylic acid groups, which were formed upon water addition during the neutralization step, back to anhydride groups. No absorption bands are observed within the 3000−4000 cm^{-1} region for both the K- and Zn-ionomers (not shown here), which

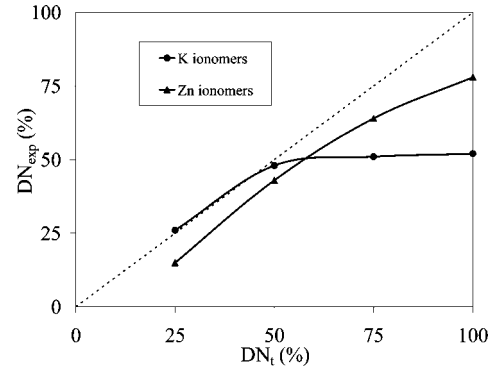

Figure 2. Experimental degree of neutralization (DN_{exp}) as a function of the targeted degree of neutralization (DN_t) for the K- and Zn-ionomers. The dashed line indicates full neutralization.

confirms the absence of absorbed water in the dry ionomers. For the K-ionomers, DN_{exp} is equal to DN_t for $DN_t < 50\%$, while a plateau value in DN_{exp} around 50% is observed for higher DN_t. Initially, the monovalent K^+ cation neutralizes the first of the two adjacent carboxylic acid groups from the hydrolyzed anhydride groups. The formation of the K-carboxylate significantly decreases the reactivity of the second carboxylic acid group toward the weak base KAc.[27] Therefore, only one of the two adjacent carboxylic acid groups is neutralized with KAc, which explains the plateau in DN_{exp} around 50%. The further increase in the intensity of the carboxylate band at 1560 cm^{-1} (Figure 1) for higher DN_t is simply due to the presence of excess KAc, since KAc has an absorption band around the same position. Neutralization with a stronger base (KOH) to a DN_t of 100% results in almost full neutralization ($DN_{exp} > 90\%$), which supports this hypothesis.

During neutralization, each dicarboxylic acid moiety is converted to a combination of a carboxylate and a carboxylic acid, so no anhydride bands are observed in the FTIR spectra of the ionomers before drying (not shown here). After drying, anhydride bands are present at 1785 cm^{-1} for the ionomers (Figure 1), which indicates that only intramolecular, cyclic anhydrides are formed and no intermolecular, acyclic anhydrides, since no absorption band at 1750 cm^{-1} is observed.[25,28,29] These results show that a reorganization of ionic groups occurs, since only acyclic anhydrides can be formed from the carboxylate−carboxylic acid moieties. The formation of cyclic anhydrides requires the conversion of two carboxylate−carboxylic acid moieties into a dicarboxylate and a dicarboxylic acid, which subsequently ring-closes to anhydride. The removal of water from the system via the applied vacuum is the driving force for anhydride and, hence, dicarboxylate formation. This is supported by observations that no anhydride bands are present in the FTIR spectra (not shown here) after drying at 170 °C without a proper vacuum. These findings demonstrate that the formation of dicarboxylates with weak bases with K^+ cations is not possible without a proper driving force.

The situation is completely different for the Zn-ionomers. DN_{exp} increases continuously but remains significantly lower than DN_t. A possible explanation for this behavior is that not all $ZnAc_2$ molecules are fully dissociated to Zn^{2+} but that $ZnAc^+$ complexes are formed as well.[30] Therefore, a fraction of the Zn atoms may be present as $ZnAc^+$ cations inside the ionic aggregates, which coordinate with one carboxylate group only, resulting in a lower DN_{exp} than DN_t. The use of the weak base $ZnAc_2$ does not result in a plateau in DN_{exp} because the remaining positive charge on the divalent Zn^{2+} cation after neutralization of the first carboxylic acid group repels the proton of the second carboxylic acid group, so a driving force for further neutralization exists. This is supported by the experi-

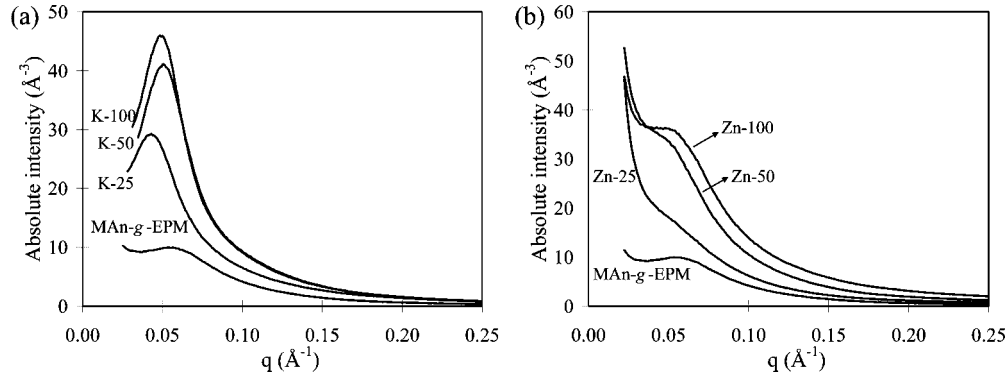

Figure 3. SAXS profiles of MAn-*g*-EPM and (a) K-ionomers and (b) Zn-ionomers with various DN_t after drying for 1 h at 170 °C under vacuum.

mental finding that drying of the Zn-ionomers for prolonged time at 100 °C under vacuum is already sufficient to convert all residual carboxylic acid groups to anhydride.

In the remainder of the text, *DN* refers to DN_t.

Morphology. The SAXS profile of the MAn-*g*-EPM precursor in Figure 3 shows a broad scattering peak around $q = 0.06$ Å^{-1}, which indicates the presence of microphase separation. The driving force for this is the large polarity difference between the polar anhydride groups and the apolar EPM chain segments. A distinct scattering peak at comparable *q* values was also observed for the low-molecular-weight MAn-*g*-EPM precursors from the previous studies, but only above a threshold value for *DG* of around 3 wt %.[19–21] The higher molecular weight for the current precursor may induce the microphase separation and explain the distinct peak despite its lower *DG* (2.1 wt %). On increasing the MAn concentration, the large polarity difference forces the anhydride groups to microphase separate into MAn-rich domains. Within these domains the MAn groups cluster together, but a significant amount of nonpolar chain segments is present.[20,21] This is very similar to the description proposed by Semenov and Rubinstein for associating polymers.[31–34]

A sharp scattering peak is observed in the SAXS profiles of the K-ionomers, while this peak is only evident as a shoulder for the Zn-ionomers (Figure 3). These results demonstrate that the microphase-separated domains remain intact upon neutralization with both cations but that the type of cation has a significant influence on the extent of phase separation. The microphase separation is well developed for the monovalent K^+ cations, resulting in a sharp scattering peak, while the use of the divalent Zn^{2+} cations results in a rather ill-defined domain, especially at lower *DN*. This is most probably related to the specific coordination behavior of Zn^{2+} cations with the dicarboxylate moieties of MAn-*g*-EPM. Grady et al. showed that Zn^{2+} cations do not coordinate to two carboxylates originating from the same hydrolyzed anhydride because the resulting bond angles and distances would be too distorted.[35] Therefore, the coordination around the Zn^{2+} cations requires two carboxylate groups from two different anhydrides. The absolute intensity of the scattering peak increases with increasing DN_t for both the K- and Zn-ionomers, which is related to the higher electron density difference between the EPM matrix and the MAn-rich domains upon the introduction of ionic interactions.

Initially, the SAXS profiles were fitted with the Yarusso–Cooper (Y–C) model, which describes the ionic domains as spherical particles with radius R_1, surrounded by a polymeric restricted-mobility layer with radius R_{CA}.[8] The particles are arranged in a liquidlike order with a distance of closest approach of $2R_{CA}$. V_p is the average volume of a volume element containing one scattering particle, so $1/V_p$ is a measure for the number of domains per volume element. Finally, $\Delta\rho$ is the electron density difference between the scattering entities and the EPM matrix. This model was successfully used to fit the SAXS patterns of the previously studied low-molecular-weight ionomers.[19] However, Figure 4 shows that the Y–C model is not capable of fitting the SAXS profiles of the current ionomers appropriately, especially at higher *q* values. Furthermore, the model does not fit the scattering peak of the Zn-ionomers very well, which is only present as a shoulder.

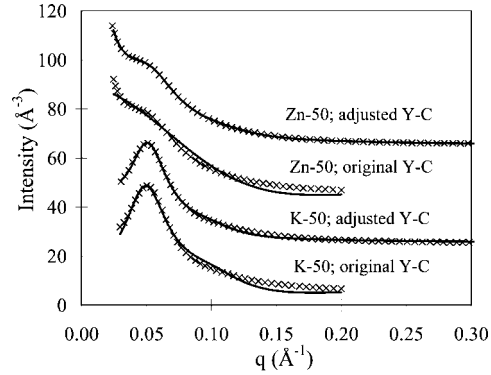

Figure 4. Best fits (—) of the experimental SAXS profiles (×) of the K-50 and Zn-50 ionomers with the original and the adjusted Y–C model. The SAXS profiles are shifted vertically for clarity.

As a first step to improve the fits, polydispersity of the domain size was taken into account.[36] For ionomers, the SAXS profiles of domains with polydisperse size distribution can be described by a model of spherical domains with a liquidlike order. The analytical Percus–Yevick equation was used for the structure factor to take the effect of interference of neighboring scattering centers into account.[37] This adjustment improves the quality of the fits significantly, but the model still cannot describe the scattering at large *q* values correctly (not shown here). The most probable explanation for this behavior is the presence of small scattering entities, e.g. (non)neutralized, non-phase-separated functional units, with sizes of a few angstroms randomly dispersed within the matrix, which results in a nonconstant background scattering from the matrix. In order to test this hypothesis, the anhydride groups of MAn-*g*-EPM were fully converted to *N*-alkylimide groups. The small difference in polarity of these groups with the EPM matrix prevents microphase separation, as observed by the disappearance of the scattering peak.[38] The SAXS profile of this material demonstrated a dependency of the intensity on $q^{-\alpha}$ with α very close to unity in the explored *q* range, which suggests the presence of some residual scattering from small structures in the matrix.[39] Therefore, such a background shape was introduced in our model.

Table 1. Parameters from the Best Fit of Eq 6 for MAn-*g*-EPM and the K- and Zn-Ionomers

sample	R_1 (Å)	R_{CA} (Å)	$R_{CA} - R_1$ (Å)	V_p (Å^3)	$\Delta\rho$ (e$^-$ Å^{-3})	$\sigma(R_1)/R_1$ (Å)
MAn-*g*-EPM	17.3	44.9	27.6	3.9×10^6	0.04	0.31
K-25	26.1	63.3	37.2	5.3×10^6	0.08	0.25
K-50	23.4	56.1	32.7	3.3×10^6	0.13	0.30
K-100	24.8	58.2	33.4	3.4×10^6	0.33	0.31
Zn-25	18.0	47.9	27.9	2.7×10^6	0.14	0.32
Zn-50	18.8	50.3	31.5	3.8×10^6	0.16	0.36
Zn-100	16.9	49.6	32.7	3.3×10^6	0.29	0.32

These adjustments result in the following equation for the scattered intensity assuming a distribution of domain sizes and a nonconstant matrix scattering:[40]

$$\frac{I(q)}{I_e(q)V} = I_{ionic} + I_{background} = \Delta\rho^2 \int_0^\infty \frac{1}{V_p} V_1^2 \Phi^2(qR_1) \frac{1}{1 + \frac{24\eta G(2qR_{CA})}{2qR_{CA}}} \times N(R_1)\, dR_1 + Cq^{-\alpha} \quad (6)$$

where V_1 is $^4/_3\pi R_1^3$, V_{CA} is $^4/_3\pi R_{CA}^3$, η is the sphere volume fraction, $G(2qR_{CA})$ is a function of q,[41] R_{CA}, and η. In the present work, the Weibull density function is used to describe the domain size distribution $N(R_1)$.[42] C is a scaling constant for the background scattering, and α is a factor close to unity in all cases. Finally, $\Phi(x)$ is the mathematical function

$$\Phi(x) = 3\,\frac{\sin x - x\cos x}{x^3} \quad (7)$$

This model provides excellent fits for all the scattering profiles of the ionomers over the whole q range (Figure 4), thereby confirming the presence of small scattering structures within the matrix in addition to the (large) domains. The necessity of these adjustments of the Y−C model for the current ionomers and not for the previously studied low-molecular-weight ionomers can be explained by the larger molecular weight between the functional groups and, concomitantly, the larger distance between the domains, which increases the probability that functional groups remain isolated within the matrix.

The values of the relevant fitting parameters, i.e., R_1, R_{CA}, V_p, $\Delta\rho$, and the fractional standard deviation $\sigma(R_1)/R_1$, are given in Table 1. For both the K- and Zn-ionomers, R_1 and R_{CA} increase initially as a function of *DN*, followed by a decrease at higher *DN*. These effects are much larger for the K-ionomers, which is related to the stronger microphase separation and the different coordination mechanism. The neutralization of the carboxylic acid groups and the coordination around the metal cations cause the size of the domains (R_1) to initially increase, whereas tightening of the domains at higher *DN* explains the subsequent decrease in size. The large increase in R_{CA} for the K-ionomers compared to that for MAn-*g*-EPM is due to the strong microphase separation, which anchors the corresponding chain segments tightly to the domains. This also explains the shift in the peak maximum to lower q values (Figure 3), since it was shown that R_{CA} is the main factor determining the peak position.[8,19] The relatively weak phase separation for the Zn-ionomers explains the smaller increase in R_{CA} and the small shift of the peak maximum with increasing *DN* (Figure 3). Finally, the size of the domains is much larger for the studied systems than for other types of ionomers, such as sodium- or zinc-neutralized ethylene−methacrylic acid copolymers,[43–45] as was also the case for the low-molecular-weight ionomers from the previous work.[19–21] However, R_1 for the high-molecular-weight ionomers is systematically lower than the values for the previously studied low-molecular-weight ionomers. This reflects that a smaller number of ionic groups are involved in the domains. Next to that, the $\sigma(R_1)/R_1$ parameter shows that the polydispersity of the domains in the Zn-ionomers is larger than in the K-ionomers. This is especially true for the samples with a *DN* of 25 and 50%. The polydispersity seems to be only influenced by the nature of the counterion and not by the degree of neutralization.

V_p and, hence, the estimated number of domains per volume element ($1/V_p$) are prone to errors because the presence of isolated MAn groups (possibly neutralized) in the matrix is not taken into account, but remain more or less similar, indicating that the number of domains is not affected by the degree of neutralization. $\Delta\rho$ increases with increasing *DN* compared to MAn-*g*-EPM for both cations, as expected. Unfortunately, despite the excellent fit quality, calculations of the number and fraction of ionic groups in the domains cannot be performed because the electron density of the matrix depends on the amount of ionic groups not included in the domains, which is unknown, although we know from the previous study that the domains contain a relatively large fraction of EPM chain segments.[20,21]

In conclusion, the currently studied ionomers show a different morphology than the previously studied low-molecular-weight ionomers. Small scattering entities are dispersed within the matrix in addition to the large microphase-separated, ion-rich domains.

To support this morphological picture, the effect of water absorption was also studied. The ionomers were immersed in water for several days, after which the changes in the SAXS profiles were monitored. Before looking at the ionomers, the effect of water absorption on the low- and high-molecular-weight precursors is discussed first. In a previous study on the low-molecular-weight precursor with a *DG* of 7.3 wt %, a water uptake of 11.3 wt % was reported.[35] This corresponds to four water molecules per carboxylic acid group. Concomitantly, R_1 increased from 24 to 41 Å. On the other hand, for the high-molecular-weight precursor studied here with a *DG* of 2.1 wt %, a water uptake of 2.5 wt % is found, corresponding to three water molecules per carboxylic acid group. However, only a small change in R_1 is observed, i.e., from 17 to 21 Å. This evidence strongly suggests that the water molecules are not fully accommodated in the domains, since a higher degree of swelling would be expected.

For the low-molecular-weight Zn-ionomer with a *DN* of 50%, the water uptake decreased to only 1.4 wt %, correspondingly to only 0.5 water molecules for every carboxylic acid group. Still, an increase in R_1 from 25 to 30 Å was found. For the high-molecular-weight Zn-ionomer, the water uptake is almost constant with respect to *DN*. For the Zn-ionomer with a *DN* = 50%, a water uptake of 1.4 wt % is measured, i.e., two water molecules for every carboxylic acid group. Surprisingly, no swelling of the ion-rich domains is observed, suggesting that the water molecules are equally distributed in the isolated ionic multiplets in the matrix and in the domains. Similar results are found for the K-ionomers. The effect of water has also implications on the mechanical properties, which will be discussed in a separate section.

Figure 5 shows the storage moduli as a function of the temperature for EPM, MAn-*g*-EPM, and the ionomers. The glass and rubber moduli and T_g (around −50 °C) increase for MAn-*g*-EPM compared to the parent EPM. The higher rubber plateau modulus for MAn-*g*-EPM suggests that the domains act as multifunctional physical cross-links that increase the network density compared to the parent EPM. The rubber plateau is extended to higher temperatures, indicating that MAn-*g*-EPM starts to flow at higher temperatures than EPM.

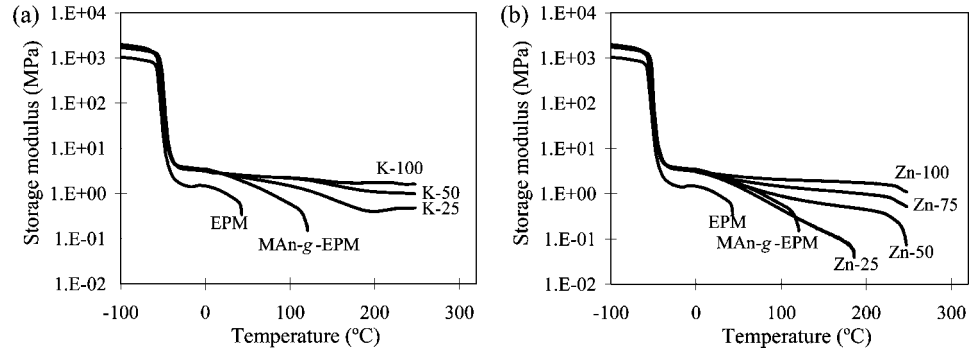

Figure 5. Storage modulus as a function of temperature for EPM, MAn-*g*-EPM, and (a) K-ionomers and (b) Zn-ionomers.

Neutralization of MAn-*g*-EPM with either K^+ or Zn^{2+} cations does not result in significant changes of the rubber plateau modulus, which indicates that the overall network density remains approximately constant. The unaffected network density upon neutralization is most probably related to the fixed molecular weight between the functional groups, which governs the distance between the domains. This agrees with the constant number of domains per volume element ($1/V_p$). However, the characteristic lifetime of the interacting groups within the domains becomes longer upon replacing the relatively weak polar interactions between the anhydride groups with ionic interactions, that persist to higher temperatures, as indicated by the extended rubber plateau. The K-ionomers have a broader plateau than the Zn-ionomers, especially at lower *DN*, which confirms that the ionic associations are stronger for the K-ionomers.

The DMTA results demonstrate that the rubber plateau and, hence, the ionic network persist to temperatures above 250 °C with the applied experimental conditions. Nevertheless, the Zn- and K-ionomers could be repeatedly compression molded into smooth and homogeneous films at 200 °C, without changes in the mechanical properties, except the K-75 and K-100 ionomers, for which the extremely strong ionic interactions prevent sufficient flow. The fact that ionomers can usually be melt processed under low shear conditions, such as compression molding,[46,47] despite the persisting presence of the ionic network,[48] is generally attributed to the occurrence of "ion hopping", as originally proposed by Cooper.[49] After a certain characteristic lifetime, the ionic groups can leave an ionic multiplet and diffuse or "hop" to another multiplet, thereby allowing stress relaxation of the chain segments connected to the ionic group. In our materials, this process can take place within the same microphase-separated domain or between different domains, although the last process is unlikely. Ionomers can flow via this mechanism without breaking all their ionic associations simultaneously.

Mechanical Properties. The previous section showed that microphase-separated domains are formed for the MAn-*g*-EPM precursor and the ionomers and that the extent of microphase separation is influenced by DN and the type of cation. This section presents the effects of these parameters on the mechanical properties. Figure 6 shows representative tensile curves for MAn-*g*-EPM and the prepared ionomers, while Table 2 gives the average values of the tensile strength (*TS*), the elongation at break (*EB*), and the compression sets (*CS*) at room temperature (CS_{23}) and at 70 °C (CS_{70}). Note that *CS* is a measure for the elasticity and has a value of 0% for an ideally elastic material and of 100% for a fully plastic material. Finally, Table 3 shows the properties of the previously studied low-molecular-weight Zn-ionomers.[19,21] Unfortunately, no K-ionomers based on the low-molecular-weight precursor were studied.

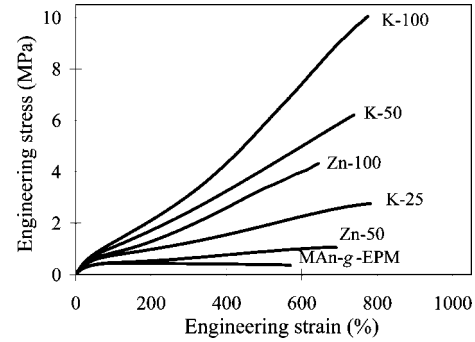

Figure 6. Representative tensile curves for MAn-*g*-EPM and the K- and Zn-ionomers.

Table 2. Mechanical Properties of MAn-*g*-EPM and the K- and Zn-Ionomers

sample	*DN* (%)	*TS* (MPa)	*EB* (%)	CS_{23} (%)	CS_{70} (%)
MAn-*g*-EPM	0	0.4	560	88	100
K-25	25	2.7	760	36	78
K-50	50	5.5	680	30	64
K-100	100	9.9	820	15	39
Zn-50	50	1.0	660	51	83
Zn-100	100	4.5	680	22	54

Table 3. Mechanical Properties of Zn-Ionomers Based on a MAn-*g*-EPM Precursor with $M_n = 11$ kg/mol and $DG = 7.3$ wt % [19,21]

DN (%)	*TS* (MPa)	*EB* (%)	CS_{23} (%)	CS_{70} (%)
0			48	100
10	1.2	270	44	92
25	1.9	270	37	65
50	1.2	170	26	43
75	1.4	150	21	35
100	1.7	140	16	31

The properties of the current ionomers are significantly affected by both the *DN* and the type of cation. The changes in *CS* with increasing *DN* are similar to those for the low-molecular-weight Zn-ionomers, whereas the trends in *EB* are completely different. The increase in *TS* with increasing *DN* is related to the increased resistance against deformation, while the increasing strength of the ionic cross-links causes the decrease in CS_{23} and CS_{70}. The different trends in *EB* can be explained with the help of the aforementioned "ion hopping" mechanism,[48] which allows ionic groups to be pulled out of the ionic aggregates within the domains under deformation and causes stress relaxation of the corresponding chain segments. The ionic groups can re-form ionic interactions and contribute to the network upon entering other multiplets in the same domain or another domain, thereby preventing premature failure and resulting in higher *EB* and higher *TS*. For the low-molecular-

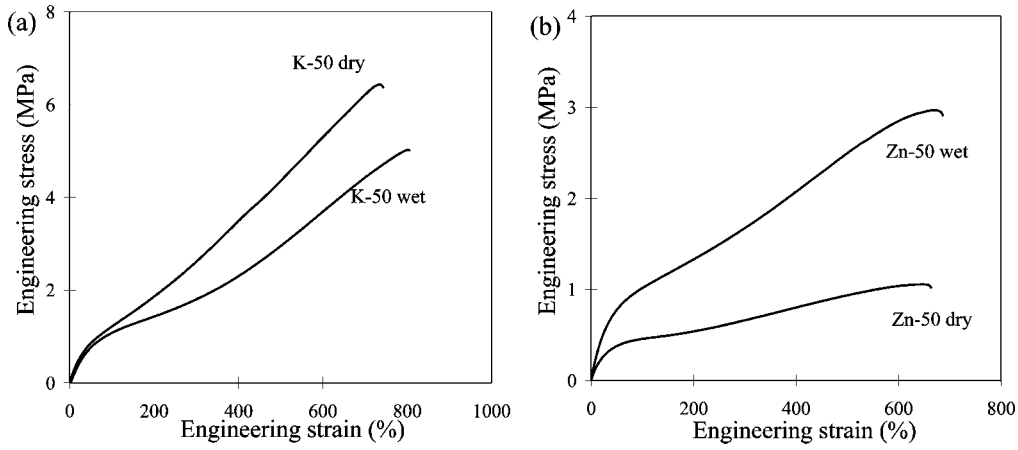

Figure 7. Representative tensile curves for (a) K-50-ionomers and (b) Zn-50-ionomers before ("dry") and after ("wet") water absorption.

weight Zn-ionomers with higher *DG*, the ionic interactions become very strong, which prevents ion hopping to a larger extent for higher *DN*. Instead, microcavities are formed within the matrix once the stress level becomes too high, leading to macroscopic failure. This explains the decrease in *EB* for this series of ionomers. For the current ionomers, especially for the Zn-ionomers, the aggregates are relatively weak and hopping can occur at any *DN*. The constant molecular weight between the functional groups may explain the constant *EB* with increasing *DN* for the current ionomers and the different trends than for the previously studied low-molecular-weight ionomers.

Another important observation is the large difference in properties between the K- and Zn-ionomers, the K-ionomers having better tensile properties and elasticity compared to those of the Zn-ionomers at similar *DN*. The previous work on the low-molecular-weight ionomers also demonstrated better tensile properties for monovalent cations, such as K^+, than for divalent cations, such as Zn^{2+}, although the differences were not so large.[19] These observations for MAn-*g*-EPM-based ionomers are different from general observations that Zn-ionomers have superior mechanical properties compared to ionomers with monovalent cations.[50,51] The poorer properties for the current Zn-ionomers are caused by the lower degree of phase separation, as detected by SAXS (see Figure 3).

Finally, a comparison of Tables 2 and 3 shows that the current K- and Zn-ionomers have significantly higher *TS* and *EB* compared to those of the low-molecular-weight Zn-ionomers, while CS_{23} and CS_{70} are higher, indicating a lower elasticity. For conventionally cross-linked elastomers, an increase in cross-link density generally results in a decrease of *EB* and *CS* and a maximum in *TS*.[52] The larger molecular weight between functional groups and, hence, the lower network density for the current ionomers compared to those of the low-molecular-weight ionomers partially explain their higher *EB* and higher *CS*. For the low-molecular-weight ionomers with their high network density, the optimum in *TS* is most probably passed, which may explain the lower *TS* compared to the current ionomers. Another important difference is that, for the currently investigated materials, the molecular weight between the functional groups is substantially higher than the molecular weight between entanglements, M_e, of the ethylene/propylene copolymer, while for the previously studied low-molecular-weight systems, the molecular weight between the functional groups was close to M_e.

The effect of water on the tensile properties was also studied. The ionomers were immersed in water for several days, after which the tensile properties were measured. The general observation in ionomer literature is that high levels of water absorption have a plasticizing or even disruptive effect on ionic aggregates or multiplets and negatively influence the ionomer properties.[53,54] Figure 7 compares representative tensile curves for selected K- and Zn-ionomers before and after water absorption. The average values of *TS* and *EB* are given in Table 4. The effect of water absorption on the tensile properties for the K-ionomers is different from that for the Zn-ionomers. The tensile properties of the K-ionomers deteriorate significantly upon water saturation. For the Zn-ionomers, on the other hand, the tensile properties improve upon water absorption, as *TS* increases without significant changes in *EB*.

Table 4. Tensile Properties of MAn-*g*-EPM and K-50 and Zn-50 Ionomers before ("Dry") and after ("Wet") Water Absorption

	"dry" materials		"wet" materials		
	TS (MPa)	*EB* (%)	*TS* (MPa)	*EB* (%)	water uptake (wt %)
K-50	5.5	680	4.9	780	1.5
Zn-50	1.0	660	2.9	670	1.4

Water absorption can induce two competing effects. One is that part of the absorbed water opens the residual anhydride rings of the ionomers to yield two carboxylic acid groups, giving these non-neutralized groups the capability to form hydrogen bonds, especially at low *DN*, which improves the strain hardening. The second effect is related to the promotion of the acid−cation exchange relaxation mechanism as proposed by Vanhoorne and Register.[45] The acid−cation exchange mechanism has a negative impact on the strain hardening. As discussed earlier, the water resides both within the isolated polar multiplets in the matrix and in the microphase-separated domains. The different effect of water on the K- and Zn-ionomers can now be explained on the basis of these two opposite effects. In the K-ionomers, where the degree of phase separation is higher, i.e., regions with a higher concentration of the carboxylic acid and cations, the acid−cation exchange mechanism is the dominating effect. Correspondingly, the strain hardening is lowered by the absorption of water. For the Zn-ionomers, on the contrary, the acid−cation exchange process is strongly reduced, as also observed by Vanhoorne and Register for Zn−ethylene−methacrylic acid ionomers,[45] and the additional hydrogen-bonding effect dominates.

Conclusions

In this work, ionic TPEs based on high-molecular-weight MAn-*g*-EPM were obtained via the neutralization of hydrolyzed MAn-*g*-EPM to various *DN* and with K^+ and Zn^{2+} as metal cations, resulting in ionomers with dicarboxylate

functionalities. The weak KAc base can only neutralize one of the two adjacent carboxylic acid groups, resulting in a plateau in DN_{exp} around 50%, due to the lowered reactivity of the second carboxylic acid after neutralization of the first acid. Neutralization of the second carboxylic acid is possible in the Zn-ionomers due to the remaining positive charge on the Zn^{2+} cations, although the presence of some $ZnAc^{+}$ cations prevents full neutralization.

The observed differences in the morphology in comparison to the previously studied ionomers based on low-molecular-weight MAn-*g*-EPM are mainly related to the molecular weight between functional groups and not to the number of functional groups per chain (in both cases $\Omega \approx 8$). This increases the probability that the matrix contains a considerable fraction of multiplets.

Unlike in many studied ionomers, in which the functional groups form clusters of multiplets, the morphology of the current ionic TPEs is governed by microphase separation in the MAn-*g*-EPM precursor. To successfully fit the SAXS data, two modifications to the original Y−C model were introduced. First, the polydispersity in the size of the domain was taken into account. Second, but even more important, was the introduction of a nonconstant matrix scattering in order to describe the contribution of isolated functional groups and multiplets, randomly dispersed within the EPM matrix, in addition to the microphase-separated domains. Unfortunately, the model does not quantify the number of multiplets and domains, and concomitantly, the number of ionic groups in the domains remains unknown.

The type of cation used for neutralization has an important influence on the ionomer morphology. Better microphase separation occurs in the K-ionomers, while the particular coordination behavior of Zn^{2+} cations, requiring two carboxylate groups from two different anhydride groups, disturbs the microphase separation to a certain extent.

The tensile properties and elasticity change dramatically upon neutralization with larger changes for the K-ionomers than for the Zn-ionomers due to the relatively weak microphase separation for the latter ionomers. The tensile properties of the current ionomers are significantly better than for the previously studied, low-molecular-weight ionomers.

The microphase-separated domains act as additional physical cross-links, resulting in an increased plateau modulus compared to the parent EPM. Neutralization with both cations increases significantly the characteristic lifetime of the interacting ionic pairs in comparison to the precursor, which allows the ionic network to stay intact at higher temperatures, without affecting the network density.

The particular morphological picture is able to describe the differences in the water absorption and in the mechanical properties with respect to the previously studied materials.

Acknowledgment. This work is part of the research program of the Dutch Polymer Institute (DPI), Eindhoven, The Netherlands, under project no. 346. We thank the staff of the DUBBLE beamline (BM26) at the European Synchrotron Radiation Facility (ESRF) in Grenoble (France) for the possibility to perform the SAXS experiments. Furthermore, we thank The Netherlands Organization for Scientific Research (NWO) for travel and research grants for the synchrotron studies.

Supporting Information Available: C_{18} alkylimide-converted MAn-*g*-EPM SAXS profile. This material is available free of charge via the Internet at http://pubs.acs.org.

References and Notes

(1) *Ionic Polymers*; Holliday, L., Ed.; Applied Science Publishers: London, 1975.
(2) *Ions in Polymers*; Eisenberg, A., Ed.; American Chemical Society: Washington, DC, 1980.
(3) *Ionomers: Synthesis, Structure, Properties and Applications*; Tant, M. R., Mauritz, K. A., Wilkes, G. L., Eds.; Chapman & Hall: London, 1997.
(4) Bonotto, S.; Bonner, E. F. *Macromolecules* **1968**, *1*, 510–515.
(5) Eisenberg, A. *Macromolecules* **1970**, *3*, 147–154.
(6) Marx, C. L.; Caulfield, D. F.; Cooper, S. L. *Macromolecules* **1973**, *6*, 344–353.
(7) MacKnight, W. J.; Taggart, W. P.; Stein, R. S. *J. Polym. Sci., Polym. Symp.* **1974**, *45*, 113–128.
(8) Yarusso, D. J.; Cooper, S. L. *Macromolecules* **1983**, *16*, 1871–1880.
(9) Eisenberg, A.; Hird, B.; Moore, R. B. *Macromolecules* **1990**, *23*, 4098–4107.
(10) *Thermoplastic Elastomers: A Comprehensive Review*; Holden, G., Legge, N. R., Quirk, R. P., Eds.; Hanser: Munich, 1996.
(11) Bagrodia, S.; Wilkes, G. L.; Kennedy, J. P. *Polym. Eng. Sci.* **1986**, *26*, 662–672.
(12) Anthony, P.; De, S. K. *J. Macromol. Sci., Polym. Rev.* **2001**, *C41*, 41–77.
(13) Agarwal, P. K.; Lundberg, R. D. *Macromolecules* **1984**, *17*, 1918–1928.
(14) MacKnight, W. J.; Lundberg, R. D. *Rubber Chem. Technol.* **1984**, *57*, 652–663.
(15) Paeglis, A. U.; O'Shea, F. X. *Rubber Chem. Technol.* **1988**, *61*, 223–237.
(16) Lundberg, R. D.; Makowski, H. S. In *Ions in Polymers*; Eisenberg, A., Ed.; American Chemical Society: Washington, DC, 1980.
(17) Datta, S.; De, S. K.; Kontos, E. G.; Wefer, J. M. *J. Appl. Polym. Sci.* **1996**, *61*, 177–186.
(18) Kurian, T.; Khastgir, D.; De, P. P.; Tripathy, D. K.; De, S. K. *Rubber World* **1995**, 41–47.
(19) Wouters, M. E. L. Ph.D. Thesis, Eindhoven University of Technology, Eindhoven, The Netherlands, 2000.
(20) Wouters, M. E. L.; Goossens, J. G. P.; Binsbergen, F. L. *Macromolecules* **2002**, *35*, 208–216.
(21) Wouters, M. E. L.; Litvinov, V. M.; Binsbergen, F. L.; Goossens, J. G. P.; van Duin, M.; Dikland, H. G. *Macromolecules* **2003**, *36*, 1147–1156.
(22) Tachino, H.; Hara, H.; Hirasawa, E.; Kutsumizu, S.; Yano, S. *J. Appl. Polym. Sci.* **1995**, *55*, 131–138.
(23) Yano, S.; Tadano, K.; Nagao, N.; Kutsumizu, S.; Tachino, H.; Hirasawa, E. *Macromolecules* **1992**, *25*, 7168–7171.
(24) Bras, W. J. *Macromol. Sci. Phys.* **1998**, *B37*, 557–565.
(25) *The Handbook of Infrared and Raman Characteristic Frequencies of Organic Molecules*; Lin-Vien, D., Colthup, N. N., Fateley, W. G., Grasselli, J. G., Eds.; Academic Press: Boston, 1991.
(26) Brozoski, B. A.; Coleman, M. M.; Painter, P. C. *Macromolecules* **1984**, *17*, 230–234.
(27) *Quantitative Organic Chemistry*; Siggia, S., Hanna, J. G., Eds.; Wiley Interscience: New York, 1979.
(28) Dauben, W. G.; Epstein, W. W. *J. Org. Chem.* **1959**, *24*, 1595–1596.
(29) Bellamy, L. J.; Connelly, B. R.; Philpotts, A. R.; Williams, R. L. *Z. Elektrochem.* **1960**, *64*, 563–566.
(30) Jeon, H. S.; Kim, J.-S. *Polym. Bull.* **2003**, *49*, 457–464.
(31) Semenov, A. N.; Rubinstein, M. *Macromolecules* **1998**, *31*, 1373–1385.
(32) Semenov, A. N.; Rubinstein, M. *Macromolecules* **1998**, *31*, 1386–1397.
(33) Semenov, A. N.; Rubinstein, M. *Macromolecules* **2001**, *34*, 1058–1068.
(34) Semenov, A. N.; Rubinstein, M. *Macromolecules* **2002**, *35*, 4821–4837.
(35) Grady, B. P.; Goossens, J. G. P.; Wouters, M. E. L. *Macromolecules* **2004**, *37*, 8585–8591.
(36) Visser, S. A.; Cooper, W. *Macromolecules* **1991**, *24*, 2584–2593.
(37) Ashcroft, N. W.; Lekner, J. *Phys. Rev.* **1996**, *145*, 83–90.
(38) Sun, C. X.; van der Mee, M. A. J.; Goossens, J. G. P.; van Duin, M. *Macromolecules* **2006**, *39*, 3441–3449.
(39) See Supporting Information.
(40) Saccà, A.; Carbone, A.; Pedicini, R.; Portale, G.; D'Ilario, L.; Longo, A.; Martorana, A.; Passalacqua, E. *J. Membr. Sci.* **2006**, *278*, 105–113.
(41) Pedersen, J. S. *Adv. Colloid Interface Sci.* **1997**, *70*, 171–210.
(42) Pedersen, J. S. *Phys. Rev. B* **1993**, *47*, 657–665.
(43) Yarusso, D. J.; Cooper, S. L. *Polymer* **1985**, *18*, 371–378.
(44) Kutsumizu, S.; Tagawa, H.; Muroga, Y.; Yano, S. *Macromolecules* **2000**, *33*, 3818–3827.
(45) Tsujita, Y.; Yasuda, M.; Takei, M.; Kinoshita, T.; Takizawa, A. Yoshimizu. *Macromolecules* **2001**, *34*, 2220–2224.
(46) Vanhoorne, P.; Register, R. A. *Macromolecules* **1996**, *29*, 598–604.
(47) Register, R. A.; Prud'homme, R. K. *Ionomers: Synthesis, Structure, Properties and Applications*; Tant, M. R., Mauritz, K. A., Wilkes, G. L., Eds.; Chapman & Hall: London, 1997.

(48) Register, R. A.; Yu, X. H.; Cooper, S. L. *Polym. Bull.* **1989**, *22*, 565–571.
(49) Cooper, W. *J. Polym. Sci.* **1958**, *28*, 195–206.
(50) Storey, R. F.; Chisholm, B. J.; Lee, Y. *Polym. Eng. Sci.* **1997**, *37*, 73–80.
(51) Bagrodia, S.; Tant, M. R.; Wilkes, G. L.; Kennedy, J. P. *Polymer* **1987**, *28*, 2207–2226.
(52) *Rubber Technology Handbook*; Hofmann, W., Ed.; Hanser Publishers: Munich, 1989.
(53) Kutsumizu, S.; Nagao, N.; Tadano, K.; Tachino, H.; Hirasawa, E.; Yano, S. *Macromolecules* **1992**, *25*, 6829–6835.
(54) Osborn, S. J.; Moore, R. B. *Polym. Prepr.* **2005**, *46*, 597–598.

MA8007509